

Hydrogen-Bonding Interactions Mediate the Phase Behavior of an A–B/C Block Copolymer/Homopolymer Blend Comprising Poly(Methyl Methacrylate-*b*-vinylpyrrolidone) and Poly(Vinylphenol)

Hsin-Fang Lee, Shiao-Wei Kuo,* Chih-Feng Huang, Jiann-Shing Lu, Shih-Chi Chan, Chih-Feng Wang, and Feng-Chih Chang*

Institute of Applied Chemistry, National Chiao Tung University, Hsin Chu, Taiwan

Received March 8, 2006; Revised Manuscript Received May 10, 2006

ABSTRACT: We have investigated a new type of A–B/C blend, formed between poly(methyl methacrylate-*b*-vinylpyrrolidone) and poly(vinylphenol) (PMMA-*b*-PVP/PVPh), that displays unusual phase behavior. In this blend, the PMMA (A) and PVP (B) blocks within the PMMA-*b*-PVP (A–B) copolymer are miscible; although PVPh (C) experiences attractive interactions ($\xi \leq 0$) through hydrogen bonding, with both the PVP and PMMA blocks, its interaction with the former block is significantly stronger than that with the latter ($\xi_{BC} \gg \xi_{AC}$). We investigated the miscibility and phase behavior of this novel A–B/C blend through the use of FTIR spectroscopy, DSC, ^{13}C CP/MAS solid-state NMR spectroscopy, and TEM. The proton spin–lattice relaxation time in the rotating frame ($T_1\rho^H$), which we determined using ^{13}C NMR spectroscopy, indicates that phase separation occurs for blends containing ca. 20–60 wt % PVPh. TEM images indicated clearly that the morphology of phase separation consists of a matrix of homogeneous mixed PVP/PVPh and micellar domains of excluded PMMA. This special phase behavior and miscibility is due mainly to the diversity of interactions that exist between the PMMA/PVPh and PVP/PVPh units.

Introduction

In recent years, there has been growing interest in the study of blends of diblock (A–B) copolymers mixed with homopolymers (C) because of the unusual phase behavior exhibited in such blending systems.^{1–10} Different kinds of A–B/C-type blend systems have been investigated extensively. One is the blend system comprising an immiscible A–B diblock copolymer ($\chi_{AB} > 0$) and a homopolymer C in which C is immiscible with block A ($\chi_{AC} > 0$) but interacts favorably with block B ($\xi_{BC} \leq 0$). Hellmann et al.^{1,2} and Kwei et al.^{8,9} have theoretically analyzed the relationships between the microphases and macrophases in a number of such blends and have compared their calculated structures with morphological observations. The other blend system comprises an immiscible A–B diblock copolymer ($\chi_{AB} > 0$) and a homopolymer C that is miscible with both blocks A and B; in such a system, C acts as a “nonselective polymer solvent” for both blocks A and B. The poly(styrene-*b*-hydroxystyrene)/poly(vinyl methyl ether) (PS-*b*-PHOST/PVME) blending system is a typical example: when the PVME content is 50% or higher, it functions as a common solvent for the two blocks and results in a single phase.⁸ Balsara et al. also demonstrated a special A–B/C blend system of poly(ethylene-*b*-propylene)/polyisobutylene (PE-*b*-PP/PIB),¹⁰ wherein χ_{AC} is positive and a decreasing function of temperature, while χ_{BC} is negative and an increasing function of temperature. These interactions lead to an order–disorder transition and macrophase separation at specific temperature range.

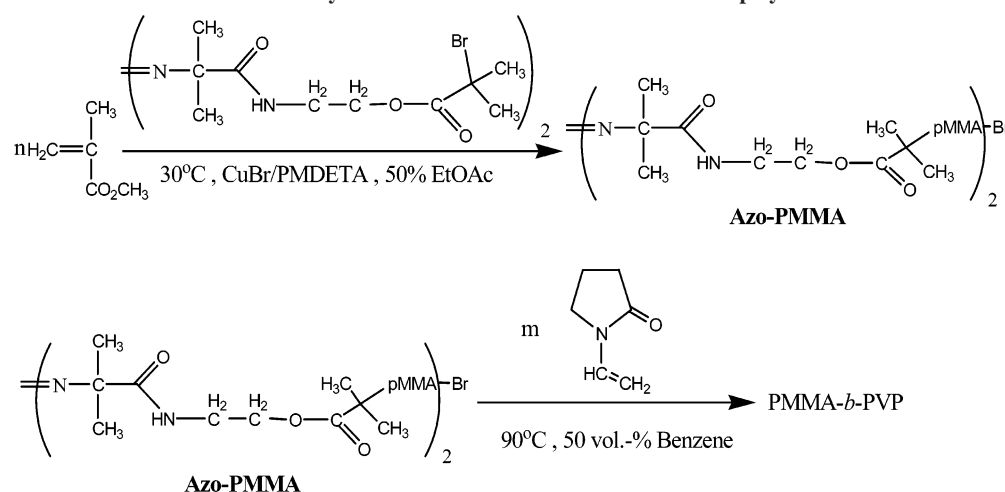
In this paper, we report a different A–B/C diblock copolymer/homopolymer system in which the value of χ_{AB} is negative (A and B are miscible) and blocks A and B both experience attractive interactions (hydrogen-bonding interactions, ξ_{AC} and ξ_{BC}) with C, but $\xi_{BC} \gg \xi_{AC}$. To investigate the miscibility and phase behavior in this blend system, we synthesized poly(methyl

methacrylate-*b*-vinylpyrrolidone) (PMMA-*b*-PVP; $M_n = 46\,000$ g/mol) and blended it with poly(vinylphenol) (PVPh). Indeed, we synthesized the PMMA-*b*-PVP block copolymer for the first time through a combination of atom transfer radical polymerization (ATRP) and conventional radical polymerization. Although ATRP has many advantages over other polymerization methods when used for block copolymerization, including a high tolerance toward a wide range of monomers and functional groups,¹¹ it has not yet been applied successfully for polymerizing vinylpyrrolidone, vinyl acetate, or olefins. One approach to overcoming this limitation is to combine ATRP with conventional radical polymerization through the use of difunctional initiators.^{12,13}

We have reported previously that PVPh is totally miscible with PVP over the entire range of blend compositions because of strong hydrogen bonding between the hydroxyl groups of PVPh and the carbonyl groups of PVP.^{14,15} In addition, Zhang et al. reported that PVPh/PMMA blends are miscible because of the hydrogen-bonding interactions that exist between PVPh's hydroxyl groups and the carbonyl groups of PMMA.^{16,17} Furthermore, according to the Painter–Coleman association model,^{18,19} the interassociation equilibrium constant of the PVPh/PVP blend ($K_A = 6000$; determined from studies of a model compound)^{20,21} is significantly higher than that of the PVPh/PMMA blend ($K_A = 37.4$).¹⁸ This result implies that the formation of hydrogen bonds between PVPh and PVP should dominate over that between PVP and PMMA in PMMA-*b*-PVP/PVPh blends.

We investigated the interactions and phase behaviors of this A–B/C-type blend of PMMA-*b*-PVP and PVPh through the use of differential scanning calorimetry (DSC), Fourier transform infrared (FTIR) spectroscopy, high-resolution ^{13}C CP/MAS NMR spectroscopy, and transmission electron microscopy (TEM). Measurements of the proton spin–lattice relaxation time in the rotating frame ($T_1\rho^H$), determined through ^{13}C NMR spectroscopic analyses, indicated that phase separation exists within blends containing 20–60 wt % PVPh. Transmission

* To whom correspondence should be addressed, E-mail: kuosw@mail.nctu.edu.tw (S-W.K.); changfc@mail.nctu.edu.tw (F-C.C.). Telephone: 886-3-5131512. Fax: 886-3-5131512.

Scheme 1. Synthesis of the PMMA-*b*-PVP Diblock Copolymer

electron microscopy images clearly indicated that the morphology of this phase transition consists of a matrix phase of mixed PVP and PVPh and micellar domains of excluded PMMA.

Experimental Section

Materials. All monomers were distilled from CaH_2 and stored under argon at $-30\text{ }^\circ\text{C}$. Triethylamine was also distilled from CaH_2 prior to use. $\text{Cu}^{\text{I}}\text{Br}$ was purified according to a literature procedure.²² All solvents were distilled prior to use. 2-Bromoisobutyryl bromide (98%, Aldrich), 2,2'-azobis[2-methyl-*N*-(2-hydroxyethyl)propionamide] (98%, WAKO), *N,N,N',N'',N'''*-pentamethyldiethylenetriamine (PMDETA; 99%, Acros), and Amberlite IR-120 (H form) cation exchange resin were used as received. Poly(vinylphenol) (PVPh; $M_n = 10\,000$) was purchased from Polyscience Inc. (USA).

Synthesis of 2,2'-Azobis[2-methyl-*N*-(2-(2-bromoisobutyryloxy)ethyl)propionamide] (AMBEP). 2-Bromoisobutyryl bromide (5.63 mL, 43.4 mmol) was added dropwise over 1 h to a stirred mixture of 2,2'-azobis[2-methyl-*N*-(2-hydroxyethyl)propionamide] (5.00 g, 17.3 mmol) and triethylamine (6.02 mL, 43.4 mmol) in CHCl_3 (150 mL) under argon in an ice bath. The reaction was then stirred at room temperature for 3 h before being washed with water ($3 \times 150\text{ mL}$) and dried (MgSO_4). After filtration, evaporation of CHCl_3 gave a white product, which was recrystallized from diethyl ether/ethyl acetate (3.83 g, 50.4%). ^1H NMR (CDCl_3) δ : 7.18 (s, 2H), 4.32 (t, 4H), 3.67 (q, 4H), 1.90 (s, 12H), 1.35 (s, 12H).

Synthesis of PMMA with a Central Azo Unit (Azo-PMMA). Azo-PMMA macroinitiator was synthesized as indicated in Scheme 1 using the ATRP technique. In a 10-mL pear-shaped flask, the AMBEP initiator (60 mg, 0.1 mmol; synthesized as described above) was degassed, and then previously degassed ethyl acetate (2 mL) was added by syringe. The mixture was stirred until the solution was homogeneous. A dry 25-mL round-bottom flask equipped with a stirrer bar and charged with $\text{Cu}^{\text{I}}\text{Br}$ (30 mg, 0.2 mmol) was degassed and then deoxygenated MMA monomer (4.5 mL, 40 mmol), ethyl acetate (2.5 mL), and PMDETA (0.13 mL, 0.6 mmol) were added sequentially; the solution was stirred for 20 min to form the Cu complex. The initiator solution was then added. This whole process was performed for 1 day in an oil bath at temperatures under $30\text{ }^\circ\text{C}$ in an argon-filled drybox. The reaction mixture was diluted 5-fold with tetrahydrofuran (THF) and then stirred with Amberlite IR-120 (H form) cation exchange resin to remove the catalyst. The mixture was then passed through an alumina column and precipitated into methanol to produce the azo-PMMA macroinitiator. The isolated yield of azo-PMMA homopolymer was 78%.

Synthesis of Poly(methyl methacrylate-*b*-vinyl pyrrolidone) Copolymer. Block copolymers of methyl methacrylate (MMA) with *N*-vinyl-2-pyrrolidone (NVP) were prepared through radical polymerization using azo-PMMA as initiator [monomers-to-azo-PMMA ratio = 200:1 (mol/mol)]. The copolymerization was

conducted in benzene at $90\text{ }^\circ\text{C}$ reflux for 24 h under an argon atmosphere. Before vacuum drying, the PMMA-*b*-PVP was precipitated repeatedly from methylene chloride solution into cold diethyl ether and purified through Soxhlet extraction with THF for 24 h to remove any unreacted azo-PMMA macroinitiator. The isolated yield of purified PMMA-*b*-PVP copolymer was 38%.

Blend Preparation. Blends of various PMMA-*b*-PVP/PVPh compositions were prepared through solution casting. DMF solutions containing a 5 wt % polymer mixture were stirred for 6–8 h and then cast on a Teflon dish. The solution was left to evaporate slowly $80\text{ }^\circ\text{C}$ for 1 day. The blend films were then dried under vacuum at $120\text{ }^\circ\text{C}$ for 2 days.

Characterization. Gel Permeation Chromatography. Molecular weight and molecular weight distributions were determined through gel permeation chromatography (GPC) using a Waters 510 HPLC, equipped with a 410 differential refractometer, a refractive index (RI) detector, and three Ultrastaygel columns (100, 500, and 10^3) connected in series in order of increasing pore size, with DMF as eluent at a flow rate of 0.6 mL/min. The molecular weight calibration curve was obtained using polystyrene standards.

Differential Scanning Calorimetry. Thermal analyses were performed using a DuPont 910 DSC-9000 controller at a scan rate of $20\text{ }^\circ\text{C}/\text{min}$ over the temperature range from 30 to $250\text{ }^\circ\text{C}$ under a nitrogen atmosphere. The sample (ca. 5–10 mg) was weighed and sealed in an aluminum pan, quickly cooled to room temperature from the first scan, and then scanned between 30 and $250\text{ }^\circ\text{C}$ at a scan rate of $20\text{ }^\circ\text{C}/\text{min}$. The glass transition temperature was taken as the midpoint of the heat capacity transition between the upper and lower points of deviation from the extrapolated glass and liquid lines.

Infrared Spectroscopy. FTIR spectra were recorded using a Nicolet Avatar 320 FTIR spectrometer and NaCl disks; 32 scans were collected at a resolution of 1 cm^{-1} . The DMF solution containing the sample was cast onto a NaCl disk and dried under conditions similar to those used in the bulk preparation. The sample chamber was purged with nitrogen to maintain film dryness.

Solid-State NMR Spectroscopy. High-resolution solid-state ^{13}C NMR spectroscopy experiments were performed at $25\text{ }^\circ\text{C}$ using a Bruker DSX-400 spectrometer operating at a resonance frequency of 100.47 MHz. High-resolution solid state ^{13}C NMR spectra were acquired using the cross-polarization (CP)/magic-angle spinning (MAS)/high-power dipolar decoupling (DD) technique, with a 90 ° pulse width of $3.9\text{ }\mu\text{s}$, a pulse delay time of 3 s, an acquisition time of 30 ms, and 2048 scans. A magic-angle sample-spinning rate of 5.4 kHz was used to avoid absorption overlapping. The proton spin–lattice relaxation time in the rotating frame ($T_1\rho^{\text{H}}$) was determined indirectly via carbon observation using a $90\text{ }^\circ\text{C}$ τ -spin lock pulse sequence prior to CP. The data acquisition was performed at delay times (τ) ranging from 0.1 to 12 ms with a contact time of 1.0 ms.

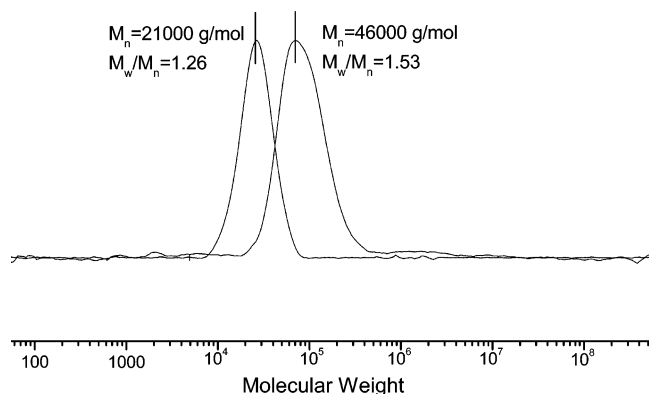


Figure 1. Molecular weight distributions of (a) poly(methyl methacrylate) ($M_w/M_n = 1.26$; $M_n = 21\,000$ g/mol) and (b) the block copolymer ($M_w/M_n = 1.53$; $M_n = 46\,000$ g/mol).

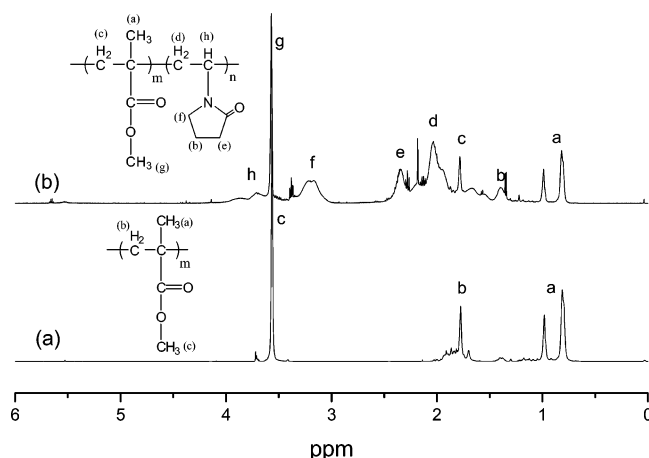


Figure 2. ^1H NMR spectra (CDCl_3) of (a) the PMMA macroinitiator and (b) the PMMA-*b*-PVP block copolymer.

Transmission Electron Microscopy. TEM analysis was performed using a Hitachi H-7500 electron microscope operated at 100 kV. Ultrathin sections of the samples were prepared using a Leica Ultracut UCT microtome equipped with a diamond knife. Slices of ca. 700 Å thickness were cut at room temperature. Some of the sliced samples were stained with the vapor from an aqueous solution of RuO_4 . The contrast between poly(methyl methacrylate) and the two other polymers increased in these samples because poly(methyl methacrylate) is selectively unstained.

Results and Discussion

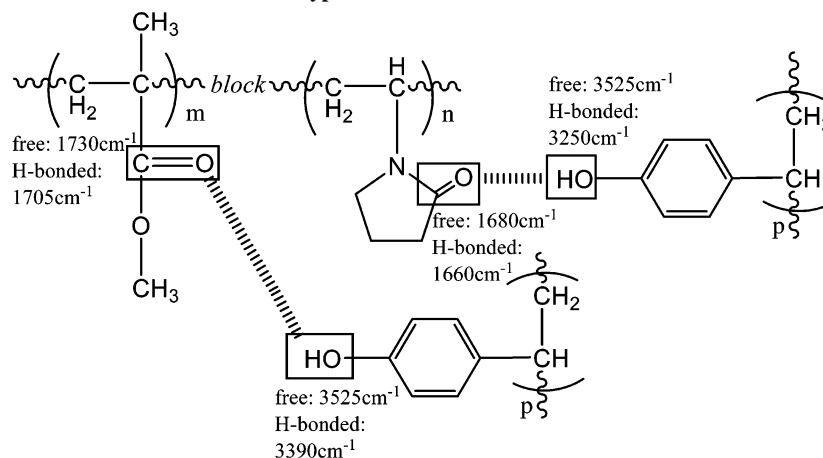
Block Copolymer Characterization. PMMA-*b*-PVP diblock copolymer was synthesized as indicated in Scheme 1. The

molecular weight distribution of the block copolymer, as measured using GPC (Figure 1), indicates that the value of M_w/M_n of PMMA was 1.26; the polydispersity of the block copolymer of methyl methacrylate and vinylpyrrolidone was 1.53. The number-average molecular weight of the PMMA block was 21 000 g/mol, and that of the block copolymer was 46 000 g/mol. Parts a and b of Figure 2 display the ^1H NMR spectra of the azo-PMMA macroinitiator and block copolymer. The latter spectrum features peaks that are characteristic of the resonances of both the PMMA and PVP blocks. The DSC analyses of the azo-PMMA macroinitiator and the PMMA-*b*-PVP copolymer were also conducted for thermal characterization. The value of T_g of azo-PMMA is 106 °C. Only one glass transition for the PMMA-*b*-PVP diblock copolymer was observed at 130 °C, indicating that the diblock copolymer is miscible between PMMA and PVP, which is in agreement with results reported in the literature.^{23,24}

Blends of PMMA-*b*-PVP and PVPh. *Fourier Transform Infrared Spectroscopic Analyses.* Scheme 2 summarizes the signals observed for the free and hydrogen-bonded hydroxyl and carbonyl vibrations in the IR spectra of both PMMA and PVP mixed with PVPh. Figure 3 displays the FTIR spectra, recorded at room temperature in the region 2700–4000 cm^{-1} (OH stretching), of PVPh and various PMMA-*b*-PVP/PVPh blends; the OH stretching signals of PMMA/PVPh (50/50) and PVP/PVPh (50/50) blends are also included for comparison. Under ambient conditions, the pure PVPh self-associated through the formation of intermolecular hydroxyl multimers. As indicated in Figure 3i, the hydroxyl band of the pure PVPh consists of two components: a relatively narrow band at 3525 cm^{-1} from the free hydroxyl groups and a broad band centered at 3360 cm^{-1} representing a wide distribution of hydrogen-bonded hydroxyl groups. Here, we focus on the variation of hydrogen-bonded hydroxyl groups. The hydroxyl groups of PVPh that form hydrogen bonds with PVP and PMMA underwent frequency shifts to 3250 (Figure 3a) and 3390 cm^{-1} (Figure 3j), respectively. From parts b–h of Figure 3, we observe in general that the hydroxyl groups of PVPh form hydrogen bonds with PVP more preferentially at lower PVPh content (i.e., the signal of the hydrogen-bonded hydroxyl groups appears mainly at 3250 cm^{-1}). At higher PVPh contents, the hydroxyl groups of PVPh also form hydrogen bonds with the PMMA blocks (i.e., the signal of the hydrogen-bonded hydroxyl groups broadens).

Figure 4 presents FTIR spectra of the carbonyl stretching region, ranging from 1630 to 1780 cm^{-1} , of PMMA-*b*-PVP and its blends at room temperature. Two types of signals for carbonyl

Scheme 2. Schematic Illustration of the Types of Interactions that Exist between PMMA-*b*-PVP and PVPh



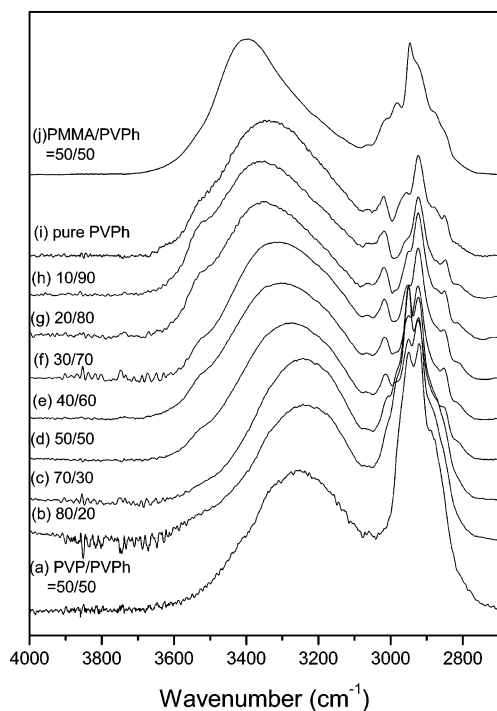


Figure 3. FTIR spectra recorded at room temperature displaying the hydroxyl stretching vibration region ($2700\text{--}4000\text{ cm}^{-1}$) for (a) PVP/PVPh (50/50), (b–h) PMMA-*b*-PVP/PVPh blends of various compositions [(b) 80/20, (c) 70/30, (d) 50/50, (e) 40/60, (f) 30/70, (g) 20/80, (h) 10/90], (i) pure PVPh, and (j) PMMA/PVPh (50/50).

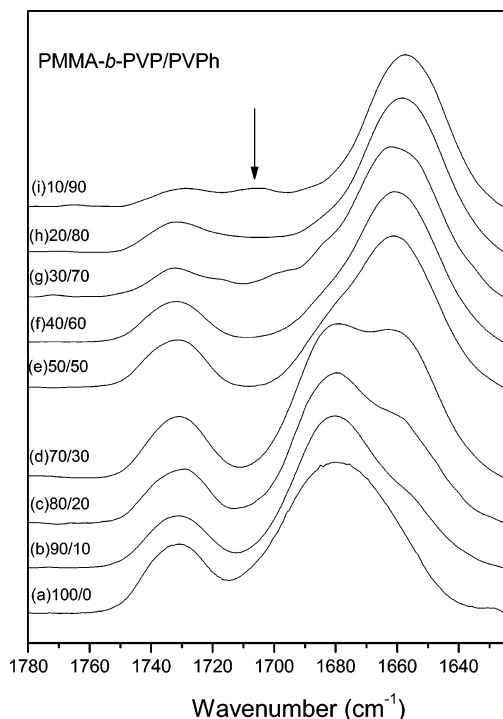


Figure 4. FTIR spectra recorded at room temperature displaying the carbonyl stretching vibration region ($1650\text{--}1780\text{ cm}^{-1}$) for PMMA-*b*-PVP/PVPh blends of various compositions: (a) 100/0, (b) 90/10, (c) 80/20, (d) 70/30, (e) 50/50, (f) 40/60, (g) 30/70, (h) 20/80, (i) 10/90.

stretching appear for the pure PMMA-*b*-PVP: the amide carbonyl stretching band of the PVP at 1680 cm^{-1} and the carbonyl stretching band of PMMA at 1730 cm^{-1} . When the PVPh content in the blend is increased, a new band appears at 1660 cm^{-1} , reflecting the presence of intermolecular hydrogen bonding between the PVP and PVPh units. In contrast, no peak

Table 1. Curve-Fitting of the Fraction of Hydrogen-Bonded Carbonyl Groups within the PMMA-*b*-PVP/PVPh Blends

polymer	PVPh content, wt %	PVP free C=O			PVP H-bonded C=O			
		ν , cm^{-1}	$W_{1/2}$, cm^{-1}	A_f (%)	ν , cm^{-1}	$W_{1/2}$, cm^{-1}	A_b (%)	f_b (%) ^a
PVP	10	1683	27	65.8	1660	31	34.2	28.5
	20	1682	25	54.9	1659	29	45.1	38.7
	30	1682	25	43.9	1659	30	56.1	49.5
	50	1681	24	17.1	1660	30	82.9	78.9
	60	1683	24	9.9	1660	30	90.1	87.5
PMMA	70	1682	25	6.7	1660	31	93.3	91.5
	60	1731	22	100				0
	70	1732	22	76.3	1700	32	23.7	17.1
	80	1731	22	61.0	1701	30	39.0	29.9
	90	1729	22	48.2	1701	29	51.8	41.7

^a f_b = fraction of hydrogen bonding.

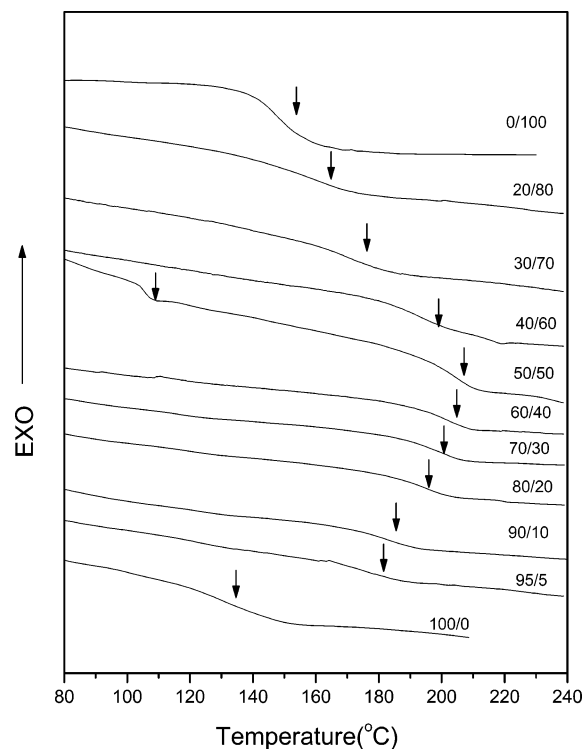


Figure 5. DSC thermograms of PMMA-*b*-PVP/PVPh blends of different compositions.

shifting and no new peaks developed for PMMA carbonyl group stretching in these blends containing a PVPh content below 60 wt %; this result implies that the PMMA carbonyl groups interact only insignificantly with PVPh when the PVPh content is less than 60 wt %. Table 1 summarizes all of these curve fitting results, i.e., the fraction of hydrogen-bonded carbonyl groups^{14,18} of PVP and PMMA as a function of PVPh content. It is clear that the PVPh hydroxyl groups begin to form hydrogen bonds with PMMA when the PVPh content is greater than 60 wt %.

These FTIR spectra are consistent with the predictions made using the Painter–Coleman association model (PCAM). According to the PCAM,¹⁸ the interassociation equilibrium constant of the PVPh/PVP blend ($K_A = 6000$, determined using a model compound) is significantly greater than that of the PVPh/PMMA blend ($K_A = 37.4$). The FTIR spectra confirm the tendency predicted by the PCAM, i.e., that the hydrogen bond formation between PVPh and PVP predominates over that between PVP and PMMA in the PMMA-*b*-PVP/PVPh blends.

Thermal Analyses. Figure 5 displays DSC thermograms of PMMA-*b*-PVP/PVPh blends in various compositions. The value

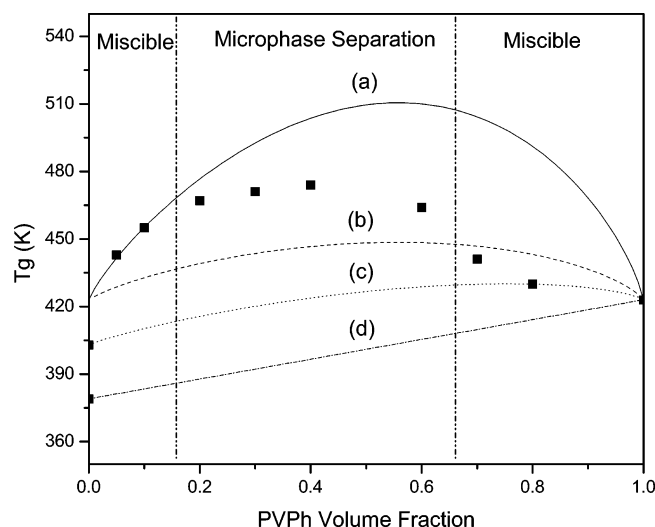


Figure 6. Plots of T_g vs composition based on (■) experimental data and (a, b) the entropy configuration models of PVP/PVPh with (a) $\gamma_{spe} = 900$ and (b) $\gamma_{spe} = 288$, (c) a combination of (b) and (d) for PMMA-*b*-PVP/PVPh, and (d) the linear rule of PMMA/PVPh.

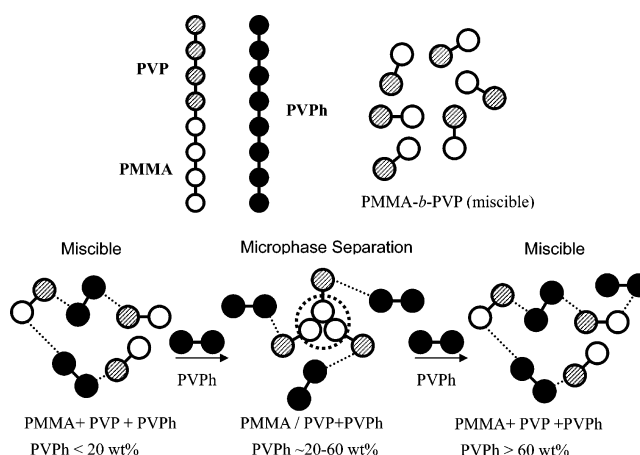
of the glass transition temperature (T_g) of PVPh is 150 °C (0/100); the PMMA-*b*-PVP block copolymer has only one glass transition, at 130 °C (100/0). For PMMA-*b*-PVP/PVPh blends, each composition exhibits a single glass transition, indicating that blends of these compositions are macroscopically miscible, except for the blend containing 50 wt % of PVPh, for which we observed two glass transitions. The lower one, at ca. 110 °C, can be assigned as reflecting a PMMA phase that had separated from the mixed phase of miscible PVP and PVPh. Presumably, this phenomenon results from the more favored formation of hydrogen bonds between PVP and PVPh than between PMMA and PVPh, as the FTIR spectra revealed.

Figure 6 displays the dependence of the value of T_g on the composition of the blends. We observed that the values of T_g were all higher than those of the individual polymers; large positive deviations indicate that strong interactions exist within the blends. The typical Fox and Gordon–Taylor equations are not suitable for describing this complicated blend system (data not shown here). Actually, the behavior of the values of T_g of PMMA/PVPh and PVP/PVPh has been reported based on the linear rule (Figure 6d)^{25,26} and configurational entropy (Figure 6b)²⁷ models, respectively. Kim et al. recently proposed²⁷ the configurational entropy model to predict the glass transition behavior of polymer blends that feature specific interactions between the components:

$$\ln\left(\frac{T_{g12}}{T_{g1}}\right) = \beta\left(1 - \gamma_{spe} \ln\left(\frac{z-1}{e}\right)\right)\left(\frac{\phi_1}{r_1} \ln \phi_1 + \frac{\phi_2}{r_2} \ln \phi_2\right) + \phi_2 \ln\left(\frac{T_{g2}}{T_{g1}}\right) \quad (1)$$

where T_{g1} , T_{g2} , and T_{g12} are the values of T_g of the pure polymers 1 and 2 and of their blend, respectively; ϕ_i and r_i are the volume fraction and degree of polymerization, respectively, of polymer i ; z is the lattice coordination number, $\beta = zR/(M_{1u}\Delta C_p)$, where R , M_{1u} , and ΔC_p are the gas constant, the molecular weight of the repeat unit, and the isobaric specific interaction of polymer 1, respectively; γ_{spe} is a proportionality constant representing the specific interactions, such as hydrogen-bonding, dipole–dipole, or ionic interactions, between the two polymers. Kim et al. reported a value of γ_{spe} of 288.1 for blends of PVP and PVPh, but this value is not appropriate for use with PMMA-

Scheme 3. Schematic Illustration of the Phase Behavior of the PMMA-*b*-PVP/PVPh Blends



PVP/PVPh blends, as indicated in Figure 6. A value of γ_{spe} of 900 fits well at relatively lower PVPh contents (<20 wt %), but increased deviation occurs between the predicted and experimental data upon increasing the PVPh content. At lower PVPh contents (<20 wt %), the value of T_g increased significantly, presumably because of nanoconfinement of PVP/PVPh with a PMMA corona phase as a result of hydrogen bonding predominantly between PVP and PVPh (Scheme 3). Upon further increasing the PVPh content (<60 wt %), segregation transition of the PMMA domain occurred to further reduce the value of T_g . Total miscibility on the macro- and microscale is expected at relatively higher PVPh contents (e.g., 80 wt %), i.e., a mixed phase of miscible PMMA, PVP, and PVPh, because the hydroxyl groups of PVPh also interact with the carbonyl groups of PMMA, as evidenced from FTIR spectroscopic analyses. As a result, the value of T_g at this composition can be predicted well using a combination of the linear rule of PMMA/PVPh (Figure 6d) and the entropy configurational model of PVP/

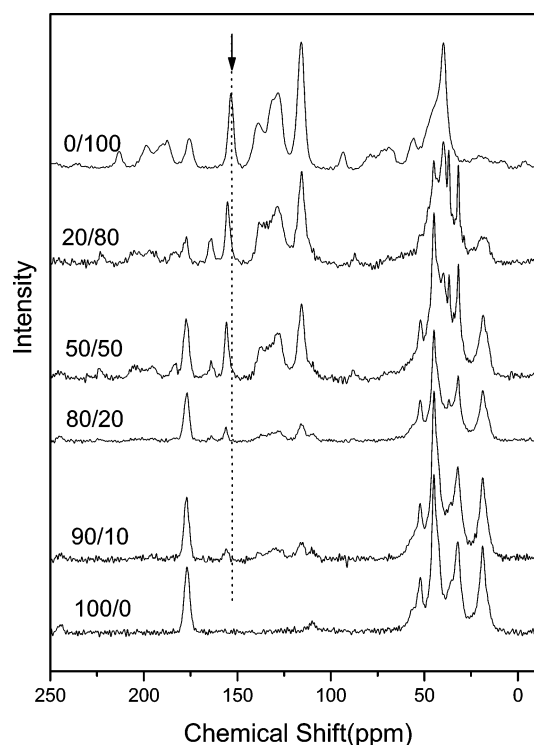


Figure 7. ^{13}C CP/MAS spectra recorded at room temperature for PMMA-*b*-PVP/PVPh blends of different compositions (weight ratios)

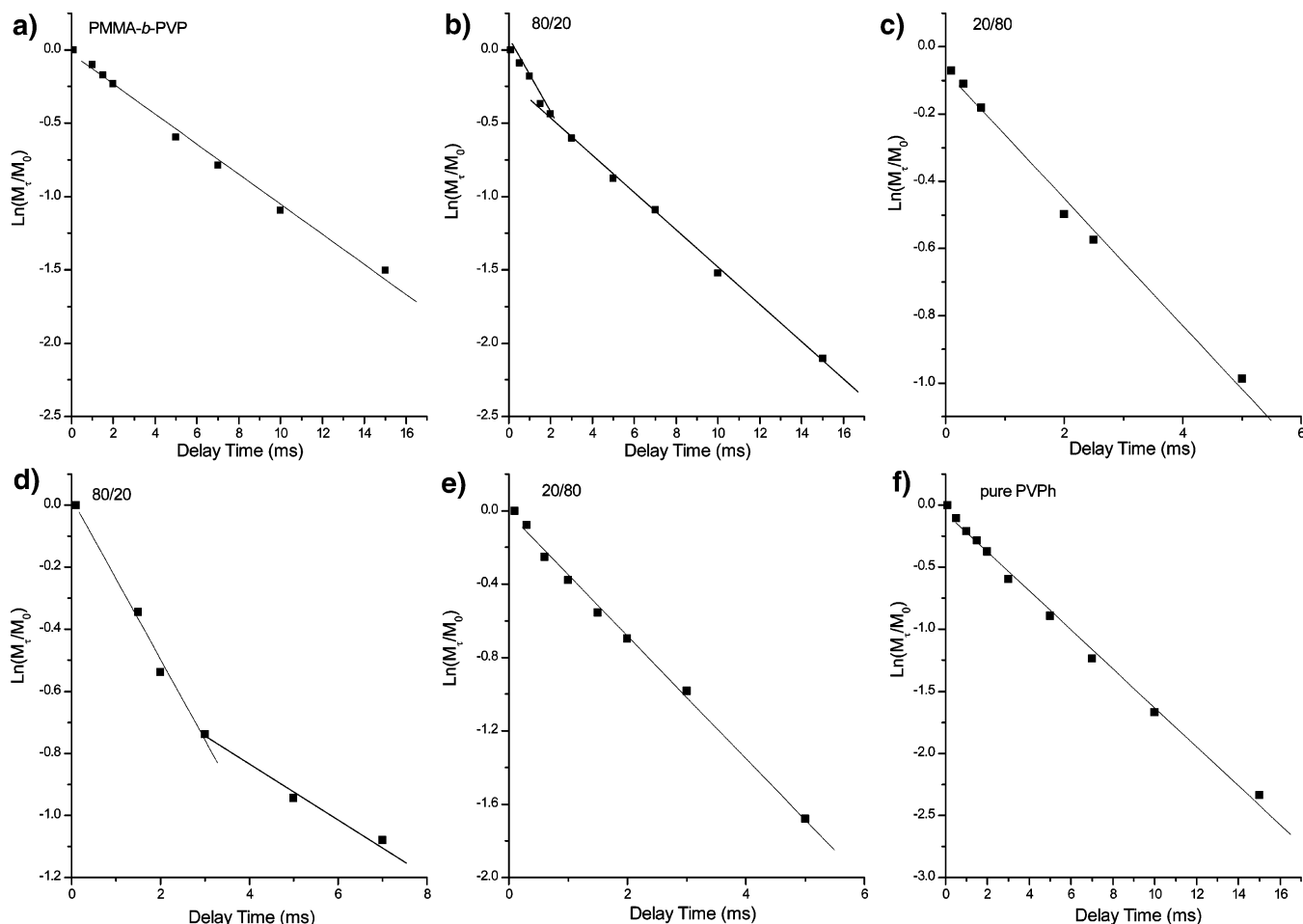


Figure 8. Semilogarithmic plots of the magnetization intensities vs delay time, with a contact time of 1.0 ms, for PMMA-*b*-PVP/PVPh blends at 177 ppm: (a) PMMA-*b*-PVP, (b) 80/20, and (c) 20/80; at 153 ppm: (d) 80/20, (e) 20/80, and (f) pure PVPh.

PVPh with a value of γ_{spe} of 288.1 (Figure 6b), as indicated in Figure 6c.

These DSC results suggest that phase transition occurs because PMMA is a significantly weaker hydrogen bond acceptor than is PVP. Added PVPh preferentially forms hydrogen bonds with PVP, rather than with PMMA, and thus, the PMMA blocks are excluded from the PVP/PVPh phase. To further investigate this phase behavior in detail, we measured the spin-lattice relaxation times ($T_1\rho^H$) in the rotating frame to examine the homogeneity of the PMMA-*b*-PVP/PVPh blends on the molecular scale (i.e., below 20 nm).

¹³C CP/MAS Solid-State NMR Spectroscopic Analyses. Solid-state NMR spectroscopy is often used to better understand the phase behavior and interactions within polymer blends.^{28–30} Figure 7 displays the ¹³C CP/MAS spectra of pure PVPh, PMMA-*b*-PVP, and PMMA-*b*-PVP/PVPh blends at various compositions. The signal for the resonance of the phenolic carbon atom of PVPh at 153 ppm underwent a gradual downfield shift upon blending with PMMA-*b*-PVP. The shift was ca. 2.5 ppm for a blend containing 80 wt % PMMA-*b*-PVP, indicating that specific interactions exist between PVPh and the block copolymer; this finding is consistent with the results of our FTIR spectroscopic analyses.

As we discussed earlier, our DSC analyses revealed that phase separation occurred for the 50/50 PMMA-*b*-PVP/PVPh blend on a scale of ca. 20–40 nm;^{31,32} we chose to study, through measurement of proton spin-lattice relaxation times in the rotating frame ($T_1\rho^H$), whether phase separation also occurred for other compositions on an even smaller scale (<20 nm). We

measured the values of $T_1\rho^H$ of the blends through delayed-contact ¹³C CP/MAS experiments, using eq 2:

$$\ln(M\tau/M_0) = -\tau/T_1\rho^H \quad (2)$$

where τ is the spin-lock time used in the experiment, and M_0 and $M\tau$ are the intensities of the peaks initially and at time τ , respectively. Parts a–f of Figure 8 present the values of $\ln(M\tau/M_0)$ plotted against τ . We estimated the homogeneities of these polymer blends through quantitative analyses based on the PMMA-*b*-PVP carbonyl carbon atom's resonance at 177 ppm (Figure 8a–c) and the PVPh phenolic carbon atom's resonance at 153 ppm (Figure 8d–f). We obtained single-exponential decays in $T_1\rho^H$ for pure PMMA-*b*-PVP, the 20/80 PMMA-*b*-PVP/PVPh blend, and pure PVPh (Figure 8a, c, e, and f), suggesting that the block copolymer, the 20/80 PMMA-*b*-PVP/PVPh blend, and PVPh are homogeneous on the scale at which spin diffusion occurs within the time $T_1\rho^H$. In contrast, the $T_1\rho^H$ decays of the carbonyl and phenolic carbon atoms' resonance of the 80/20 PMMA-*b*-PVP/PVPh blend were not single-exponential (Figure 8b and d); in addition to a main decay, there also exists a slow decaying component, indicating that two domains, with distinct mobilities, were present in this blend^{33,34} on a scale below 20 nm.

From the slopes of fitted lines, we determined the values of $T_1\rho^H$, which are listed in Table 2, for various compositions of PMMA-*b*-PVP/PVPh blends. Blends containing less than 10 wt % of PVPh display homogeneous single-exponential behavior. When the PVPh content increases to 20 wt %, nonexponential

Table 2. Values of $T_{1\rho}^H$ of the PMMA-*b*-PVP Copolymer, Pure PVPh, and Various Compositions of PMMA-*b*-PVP/PVPh Blends

PMMA- <i>b</i> -PVP/PVPh blend compositions	$T_{1\rho}^H$ (ms)	
	177 ppm	153 ppm
100/0	9.75	
90/10	12.5	
80/20	3.92/7.76	3.85/11.70
50/50	5.39/4.99	3.60/4.89
20/80	5.28	2.98
0/100		6.36

relaxation behavior occurs because the phase transits into two domains: i.e., a PMMA phase that separated from a mixed phase of miscible PVP and PVPh. At higher PVPh contents, the blends became homogeneous again as a result of hydrogen bond formation between PMMA and PVPh.

Combining results of the FTIR spectroscopic, DSC, and delayed-contact ^{13}C CP/MAS experiments, we conclude that phase transition actually began to occur when the blends contained ca. 20–60 wt % of PVPh. Furthermore, the blends became homogeneous when the PVPh content was larger than 60 wt % because hydrogen bonds began to form between the PMMA and PVPh units (from Table 1).

TEM Analyses. We visualized the morphology of the phase transition through TEM analysis of a film of the PMMA-*b*-PVP/PVPh blend (70/30). The film was stained with RuO_4 , whereupon the PVPh chain was deeply stained, the PVP chain was only lightly stained, and the PMMA chain was selectively unstained. Figure 9 indicates that two phases are present in the film of the blend. The matrix, i.e., the gray region, corresponds to a mixed phase of lightly stained PVP and deeply stained PVPh; the bright region, with formation of micellar domains, corresponds to a PMMA phase that had been excluded from the mixed phase because of its significantly weaker ability to form hydrogen bonds with PVPh. The large black regions dispersed in the matrix probably arose from imperfect staining.

Our studies of the phase behavior in these A-*B/C*-type PMMA-*b*-PVP/PVPh blends, performed using IR spectroscopy, DSC, ^{13}C CP/MAS NMR spectroscopy, and TEM, suggest that phase transition occurred for blends containing ca. 20–60 wt % of PVPh. Scheme 3 summarizes the detailed phase behavior of these PMMA-*b*-PVP/PVPh blends. Pure PMMA-*b*-PVP exhibits good miscibility between its two blocks. When ca. 20–60 wt % of PVPh was present in the blend, segregation transition

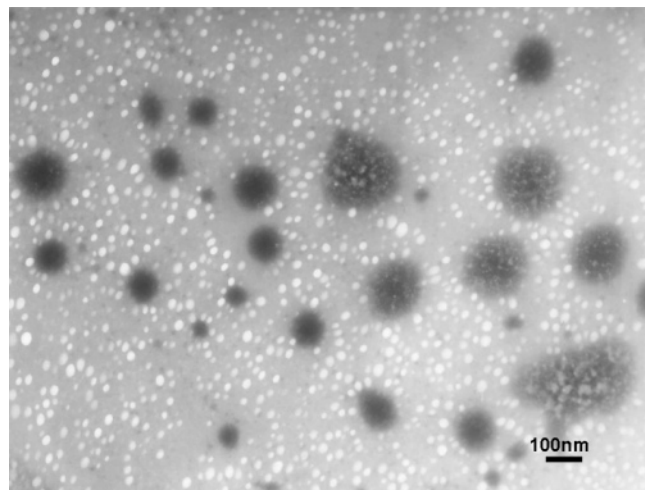


Figure 9. Transmission electron micrograph of the solution-cast film of the 70/30 (wt %) PMMA-*b*-PVP/PVPh blend stained with RuO_4 . The dark region (matrix) corresponds to a mixed phase of -PVP and PVPh; the white region (micelles) corresponds to excluded -PMMA.

occurred into domains containing a matrix of mixed PVP and PVPh and micellar domains of excluded PMMA. These blends become homogeneous again when the PVPh content was greater than 60 wt % because, under these conditions, hydrogen bonds formed between PMMA and PVPh also.

Conclusions

We have investigated the phase behavior, mediated by hydrogen-bonding interactions, of novel A-*B/C*-type PMMA-*b*-PVP/PVPh blends. We synthesized the PMMA-*b*-PVP copolymer by combining atom transfer radical polymerization with conventional radical polymerization. FTIR spectra provided evidence that the PVP carbonyl groups are significantly stronger hydrogen bond acceptors than are the PMMA carbonyl groups. Furthermore, DSC revealed that phase transition existed in this A-*B/C* blend system. FTIR and ^{13}C CP/MAS NMR spectra provided additional evidence confirming that phase transition occurred for the blends containing ca. 20–60 wt % of PVPh. TEM imaging clearly indicated that the morphology of the segregation transition consisted of a matrix of a homogeneous mixed PVP/PVPh phase and micellar domains of excluded PMMA. The blends became homogeneous again when the PVPh content was greater than 60 wt % because hydrogen bonds also formed between the PMMA and PVPh units. In conclusion, the diversity of attractive interactions (ξ) between the PMMA and PVPh and the PVP and PVPh moieties appears to be a major factor influencing the phase behavior of this A-*B/C* blend system.

Acknowledgment. This research was supported financially by the National Science Council, Taiwan, Republic of China, under contract no. NSC-94-2216-E-009-002 and Ministry of Education “Aim for the Top University” program (MOEATU program).

References and Notes

- Lowenhaupt, B.; Steurer, A.; Hellmann, G. P. *Polymer* **1991**, *32*, 1065.
- Lowenhaupt, B.; Steurer, A.; Hellmann, G. P.; Gallot, Y. *Macromolecules* **1994**, *27*, 908.
- Tucker, P. S.; Barlow, J. W.; Paul, D. R. *Macromolecules* **1988**, *21*, 2794.
- Tucker, P. S.; Paul, D. R. *Macromolecules* **1988**, *21*, 2801.
- Hashimoto, T.; Tanaka, H.; Hasegawa, H. *Macromolecules* **1990**, *23*, 4378.
- Hashimoto, T.; Kimishima, K.; Hasegawa, H. *Macromolecules* **1991**, *24*, 240.
- Tanaka, H.; Hashimoto, T. *Macromolecules* **1991**, *24*, 5713.
- Zhao, J. Q.; Pearce, E. M.; Kwei, T. K. *Macromolecules* **1997**, *30*, 7119.
- Han, Y.-K.; Pearce, E. M.; Kwei, T. K. *Macromolecules* **2000**, *33*, 1321.
- Lee, J. H.; Balsara, N. P.; Chakraborty, A. K.; Krishnamoorti, R.; Hammouda, B. *Macromolecules* **2002**, *35*, 7748.
- Matyjaszewski, K.; Xia, J. *Chem. Rev.* **2001**, *101*, 2921.
- Destarac, M.; Boutevin, B. *Polym. Prepr.* **1998**, *39*, 568.
- Paik, H.-J.; Teodorescu, M.; Xia, J.; Matyjaszewski, K. *Macromolecules* **1999**, *32*, 7023.
- Kuo, S. W.; Chang, F. C. *Macromolecules* **2001**, *34*, 5224.
- Kuo, S. W.; Chang, F. C. *Polymer* **2003**, *44*, 3021.
- Zhang, X.; Takegoshi, K.; Hikichi, K. *Macromolecules* **1991**, *24*, 5756.
- Zhang, X.; Takegoshi, K.; Hikichi, K. *Macromolecules* **1992**, *25*, 4871.
- Coleman, M. M.; Graf, J. F.; Painter, P. C. *Specific Interactions and the Miscibility of Polymer Blends*; Technomic Publishing: Lancaster, PA, 1991.
- Coleman, M. M.; Xu, Y.; Painter, P. C. *Macromolecules* **1994**, *27*, 127.
- Moskala, E. J.; Varnell, D. F.; Coleman, M. M. *Polymer* **1985**, *26*, 228.
- Hu, Y.; Motzer, H. R.; Etcheberria, A. M.; Fernandez-Berridi, M. J.; Iruin, J. J.; Painter, P. C.; Coleman, M. M. *Macromol. Chem. Phys.* **2000**, *201*, 705.
- Keller, R. N.; Wycoff, H. D. *Inorg. Synth.* **1946**, *2*, 1.

- (23) Hsu, W. P. *J. Appl. Polym. Sci.* **2001**, *81*, 3190.
- (24) da Silva, E. P.; Tavares, M. I. B. *Polym. Bull.* **1998**, *41*, 307.
- (25) Li, D.; Brisson, J. *Macromolecules* **1996**, *29*, 868.
- (26) Lin, C. L.; Chen, W. C.; Liao, C. S.; Su, Y. C. Huang, C. F. Kuo, S. W.; Chang, F. C. *Macromolecules* **2005**, *38*, 6435.
- (27) Kim, J. H.; Min, B. R.; Kang, Y. S. *Macromolecules* **2006**, *39*, 1297.
- (28) Hill, D. J. T.; Whittaker, A. K.; Wong, K. W. *Macromolecules* **1999**, *32*, 5285.
- (29) Kuo, S. W.; Chang, F. C. *Macromolecules* **2001**, *34*, 4189.
- (30) Cheung, M. K.; Wang, J.; Zheng, S.; Mi, Y. *Polymer* **2000**, *41*, 1469.
- (31) Utracki, L. A. *Polymer Alloys and Blends*; Hanser: Munich, 1989.
- (32) Guo, M. *Trends Polym. Sci.* **1996**, *4*, 238.
- (33) Tanaka, H.; Nishi, T. *Phys. Rev. B* **1986**, *33*, 32.
- (34) Stejskal, E. O.; Schaefer, J.; Sefcik, M. D.; McKay, R. A. *Macromolecules* **1981**, *14*, 275.

MA0605189